THE MICHIGAN EARTH GRID: DESCRIPTION, REGISTRATION METHOD FOR SSM/I DATA, AND DERIVATIVE MAP PROJECTIONS

John F. Galantowicz
Anthony W. England

February 1991

27396-2-T = RL-2415

Technical Report

THE MICHIGAN EARTH GRID:
DESCRIPTION, REGISTRATION METHOD FOR SSM/I DATA, AND DERIVATIVE MAP PROJECTIONS

John F. Galantowicz
Anthony W. England

Radiation Laboratory
Department of Electrical Engineering and Computer Science
University of Michigan
Ann Arbor, MI 48109-2122
Phone: (313) 763-5534
FAX: (313) 763-1503

February 1991

Report 027396-2-T

Contents

List of Figures

List of Tables

1. Introduction

In response to a task defined by the SSM/I Products Working Team (SPWT), we have developed a format and registration method for storage of global data from the Special Sensor Microwave/Imager (SSM/I) on digital media such as compact disk. This technical report describes firstly the Michigan Earth Grid, version 1b (MEG1b). MEG1b delineates a set of grid points which covers the entire Earth while retaining sample spacings similar to the spatial resolutions of the original SSM/I measurements. We show that by matching grid point spacing and spatial resolution MEG1b covers the globe with minimum storage requirements. The grid resembles an equal-area Sinusoidal projection of the earth when displayed and we show how data from the grid is readily mapped to local Sinusoidal and conformal projections.

Secondly, we present a method for resampling of SSM/I data to points on the Michigan Earth Grid that retains the spatial characteristics of the original data. The treatment is based upon Backus-Gilbert theory and follows the work of Stogryn [1] and Poe [2]. The process involves interpolation to increase the density of antenna temperature measurements in the satellite swath reference frame as if the additional samples had been made by the satellite radiometer itself—i.e., the beam patterns and spatial resolutions of the interpolated data approximate those of the original samples. The implementation requires no *a priori* knowledge of earth surface spatial or spectral characteristics. Assignment of radiobrightness values to points on MEG1b is performed by nearest-neighbor registration of the interpolated data. Because our interpolated data set is effectively grossly oversampled, nearest-neighbor registration introduces little error.

2. Michigan Earth Grid

2.1. General Description

MEG1b grid points are arranged in uniformly spaced rows parallel to the equator, and the spacing between points in a row is identical to the spacing between rows. Hence, only the 0^{th} column of every row will fall on a common meridian. That is, although grid points can be mapped to latitude according to their row alone, the mapping of a point to longitude is a function of its row. When displayed, this type of grid results in a Sinusoidal projection of the globe. Other local displays of the data will require a resampling program to map MEG1b into useful projections, to be described in section 4.

MEG1b actually defines three grids, the sparsest of which has points approximately 40 km apart at the equator. This grid point spacing closely matches the effective field of view (EFOV) of the 19 and 22 GHz channels but is approximately twice and four times the EFOV of the 37 and 85 GHz channels, respectively. Hence, grids for the 37 and 85 GHz channels are defined with precisely twice and four times the number of points in the 19/22 GHz grid, yielding grid point spacings of about 20 and 10 km at the equator, respectively. 1/297 flattening of the oblate ellipsoidal Earth will render the grid points near the poles somewhat closer together than at the equator.

MEG1b is based upon an equatorial, right-hand spherical coordinate system with $\phi = 0°$ at the equator and $\lambda = 0°$ at the 0° meridian (corresponding to latitude and longitude). 0° was chosen as the central meridian because its location is easily visualized and because the

resulting seam in the grid at 180° does not cross a major land mass. The mid-point in each row will be on the 0° meridian with points numbered positive to the east and negative to the west. The spacing between the the last point in a row and the first will vary among rows between 0 and 40, 20 or 10 km, depending on the grid, and there will be some overlapping at the 180° meridian.

2.2. Point Numbering for 19/22 GHz Grid

Assuming an equatorial radius of 6,378.388 km, the Earth equatorial circumference is $C_E = 40{,}076.594$. A 40 km grid point spacing then yields 1002 points. Rounding this off to 1000 columns—with the -500^{th} column at the 180° meridian and the $+499^{th}$ column located just to the west of it—yields a 40.077 km point spacing at the equator. Similarly, a 40.077 km row spacing yields 501 rows, including a point at both poles. If we designate a point on the 19/22 GHz grid by its row number, n, and column number, m, then

$$-N \le n \le N$$

where N = 250, and,

$$-M_n \le m \le (M_n - 1)$$

where $M_{n=0} = 500$ on the equator. For other than the equatorial row (n=0):

$$M_n = M_0 - \mathrm{INT}[\, M_0 (1 - \cos \phi_n)] = -\mathrm{INT}[\, - M_0 \cos \phi_n]$$

where $\phi_n = \frac{\pi n}{2N}$ is latitude, and the function INT means the largest integer that is less than or equal to the argument, and is not equivalent to the FORTRAN intrinsic function INT.

2.3. Point Numbering for 37 and 85 GHz Grids

To designate points on the 37 and 85 GHz grids we will use the superscripts $()^{37}$ and $()^{85}$. Using grid point spacings of 20.0385 and 10.01925 km to define the 37 and 85 GHz grids in a manner similar to the 19/22 GHz grid, we have the points (n^{37},m^{37}) and (n^{85},m^{85}) such that:

a) $-N^{37} \le n^{37} \le N^{37}$, $N^{37} = 500$,
b) $-M^{37}_{n=0} \le m^{37} \le (M^{37}_{n=0} - 1)$, $M^{37}_{n=0} = 1000$,
c) $-N^{85} \le n^{85} \le N^{85}$, $N^{85} = 1000$,
d) $-M^{85}_{n=0} \le m^{85} \le (M^{85}_{n=0} - 1)$, $M^{85}_{n=0} = 2000$.

As described in section 2.5, each 19/22 GHz grid point is associated with four 37 GHz points and sixteen 85 GHz points in storage. The following simple rules relate points on the 37 or 85 GHz grids to the corresponding points on the 19/22 GHz grid:

e) $n = \mathrm{INT}[(n^{37}+1)/2]$, $n = \mathrm{INT}[(n^{85}+3)/4]$,
f) $m = \mathrm{INT}[m^{37} / 2]$, $m = \mathrm{INT}[m^{85} / 4]$.
g) $M^{37}_n = 2\, M_n$,
h) $M^{85}_n = 4\, M_n$.

In general, a 19/22 GHz grid point is associated with the higher frequency points located below and to the right of it as viewed on the Sinusoidal projection.

2.4. Mapping Grid Points to Latitude and Longitude

The location of each MEG1b point, P^i_{nm}, where the superscript $()^i$ represents either the 19/22, 37 or 85 GHz grids, is uniquely mapped from (n^i,m^i) to (lat,lon) by:

$$\text{Lat}(P^i_{nm}) = 90\, n^i / N^i \text{ , in degrees N if } > 0, \text{ degrees S if } < 0,$$

$$\text{Lon}(P^i_{nm}) = 360\, m^i \Delta x^i/(C_E \cos \phi^i_n)] \text{ , in degrees W if } <0, \text{ degrees E if } >0,$$

where: $\phi^i_n = \text{Lat}(P^i_{nm})$,

Δx^i = Grid point spacing $\approx$ 40, 20, 10 km.

These equations can be inverted to provide a unique mapping from (lat,lon) to (n^i,m^i).

2.5. Digital Storage Format

In order to facilitate quick analysis of gross spectral characteristics, data from the three grids which are co-located and carry the same time tag should be stored together. We suggest defining a storage cell to contain all the radiobrightness data associated with a 19/22 GHz grid point, as described in section 2.3. In addition, the storage cell should contain a one byte time tag and an (n,m) integer coordinate set to readily locate the cell on the 19/22 GHz grid. With one byte for each of 43 radiobrightnesses, a time tag and two coordinates, and assuming that we record at least two satellite passes per day, then each storage cell will be a linear array with 90 one-byte elements. One way to organize the data in a cell is shown in Table 1.

Table 1.

	Byte Number	
Data type:	First Pass:	Second Pass:
Row, n	1	
Column, m	2	
Time tag	3	47
19 GHz, V-pol.	4	48
19 GHz, H-pol.	5	59
22 GHz	6	50
4 x 37 GHz, V-pol.	7-10	51-54
4 x 37 GHz, H-pol.	11-14	55-58
16 x 85 GHz, V-pol.	15-30	69-74
16 x 85 GHz, H-pol.	31-46	75-90

The higher frequency data are put in byte numbers according to their position relative to the corresponding 19/22 GHz grid point. For example, the 37 and 85 GHz vertically polarized first pass data would map to byte numbers as shown in Figures 1a and 1b, respectively. Data in bytes 7 and 15—here marked by X's—are co-located geographically with those in bytes 4, 5 and 6. Because there is only one grid point at the south pole irrespective of channel, the extraneous bytes there will be null sets.

Figure 1: Example of mapping data from MEG1b byte numbers to relative grid positions.

a) 37 GHz, V-pol.

7 x 8 •

9 • 10•

b) 85 GHz, V-pol.

15x 16• 17• 18•

19• 20• 21• 22•

23• 24• 25• 26•

27• 28• 29• 30•

2.6. Total Digital Storage Requirement

Data storage based upon a MEG1b format does not constitute a compression of the original radiometric data because the resampled data closely reflect the original spatial resolutions. However, because the MEG1b grid points are fixed with respect to the Earth, their locations need not be recorded with each data cell as geolocation must be for data stored in a satellite reference frame. All that is needed is the (n,m) integer coordinate set associated with each cell, as described above. The total byte requirement per day comes to 90 x N_{tot} bytes, where N_{tot} is the total number of cells in MEG1b. N_{tot} can be approximated by:

$$N_{tot} = \frac{\text{Approx. area of Earth's surface}}{\text{Area associated with each cell}}$$

$$= \frac{4\pi R^2}{40.077^2}$$

$$= 318{,}304 \text{ cells.}$$

That is, the total daily byte requirement becomes: 90 x 318,304 = 28.65 Mbytes/day. If a CD holds 650 Mbytes, then 1 CD covers about 23 days. If Northern and Southern Hemisphere data are produced on separate disks, and with some data compression so that null data (gaps of no coverage or one pass coverage) do not take up the full 90 byte allotment for each cell, then it may be possible that two months of one satellite, one hemisphere, two pass coverage could be recorded on one CD.

3. Processing SSM/I Data for Storage

3.1. Introduction

Recent improvements in the geo-location of radiobrightness data (i.e., Poe [3]) justify care in resampling the SSM/I data to a common Earth reference grid. The geometry of spaceborne microwave radiometry makes it impossible to map the data to a useful projection by nearest-neighbor resampling without significant loss in accuracy. In mapping radiobrightness measurements to a common reference system, such as the Michigan Earth Grid, the resampling process should preserve the original spatial resolution and avoid the introduction of spatial or spectral processing artifacts. These objectives can be met by

increasing the density of the original data with an interpolation filter and performing nearest-neighbor resampling with minimal re-registration from the dense data field.

The interpolation filter could be described as optimal if interpolated data at a particular point duplicates the measurement which would have been made had the radiometer made the measurement itself. Such a method for closely approximating the "optimal" interpolation of radiometer data is described by Poe [2] and is based on the application of Backus-Gilbert matrix inversion methodology as discussed in Stogryn [1]. Our objective is to demonstrate Poe's interpolation method and nearest-neighbor resampling to map SSM/I data in the satellite reference frame to the MEG1b reference frame while retaining the spatial resolution and the antenna beam pattern of the original data.

3.2. Interpolation to Higher Sample Density

3.2.1. Theory

This section is derived primarily from Poe [2] with additions from Stogryn [1]. The SSM/I views the earth with the geometry shown in Figure 2 (modified from Figure 2.8 in the SSM/I User's Guide[4]). In terms of the instantaneous antenna gain, $G(\hat{s}_0(t'),\hat{s}(t'))$, the antenna temperature , $T_A(\hat{s}_A)$, measured in the direction $\hat{s}_A$, is given by:

$$T_A(\hat{s}_A) = \int_{-\infty}^{+\infty} dt' h(t') \iint_E d\Omega G(\hat{s}_0(t'),\hat{s}(t')) T_B(\vec{\rho},\hat{s}(t'),t') \tag{1}$$

where $\hat{s}_0(t')$ is the instantaneous boresight direction of the antenna, $\hat{s}(t')$ is the unit vector from the antenna in the direction of the solid angle $d\Omega$, $\vec{\rho}$ is the position vector of a spherical earth surface coordinate system, and h is the impulse response of the radiometer receiver low-pass filter. The areal region of integration encompasses the entire surface of the earth intercepted by $\hat{s}(t')$. Note that both h and G are normalized such that $\int_{-\infty}^{+\infty} dt\, h = 1$ and $\int_E d\Omega G = 1$. The effective antenna pointing direction, $\hat{s}_A$, is given by

$$\hat{s}_A = \int_{-\infty}^{+\infty} dt' h(t') \hat{s}_0(t') = \frac{1}{\tau} \int_{-\frac{1}{2}}^{+\frac{1}{2}} dt' \hat{s}_0(t') \tag{2}$$

where h has been replace by integration over τ.

The differential solid angle, $d\Omega$, can be replaced by the corresponding differential area of the earth's surface according to:

$$d\Omega = \left[\frac{-\hat{s}(t') \cdot \hat{\rho}}{s^2(t')} \right] dA \tag{3}$$

Exchanging the time and space integrations, we can rewrite (1) as:

$$T_A(\vec{\rho}_A) = T_A(\hat{s}_A) = \frac{1}{\tau} \iint_E dA \int_{-\frac{1}{2}}^{+\frac{1}{2}} dt' \left\{ G(\hat{s}_0(t'),\hat{s}(t')) \left[\frac{-\hat{s}(t') \cdot \hat{\rho}}{s^2(t')} \right] T_B(\vec{\rho},\hat{s}(t'),t') \right\} \tag{4}$$

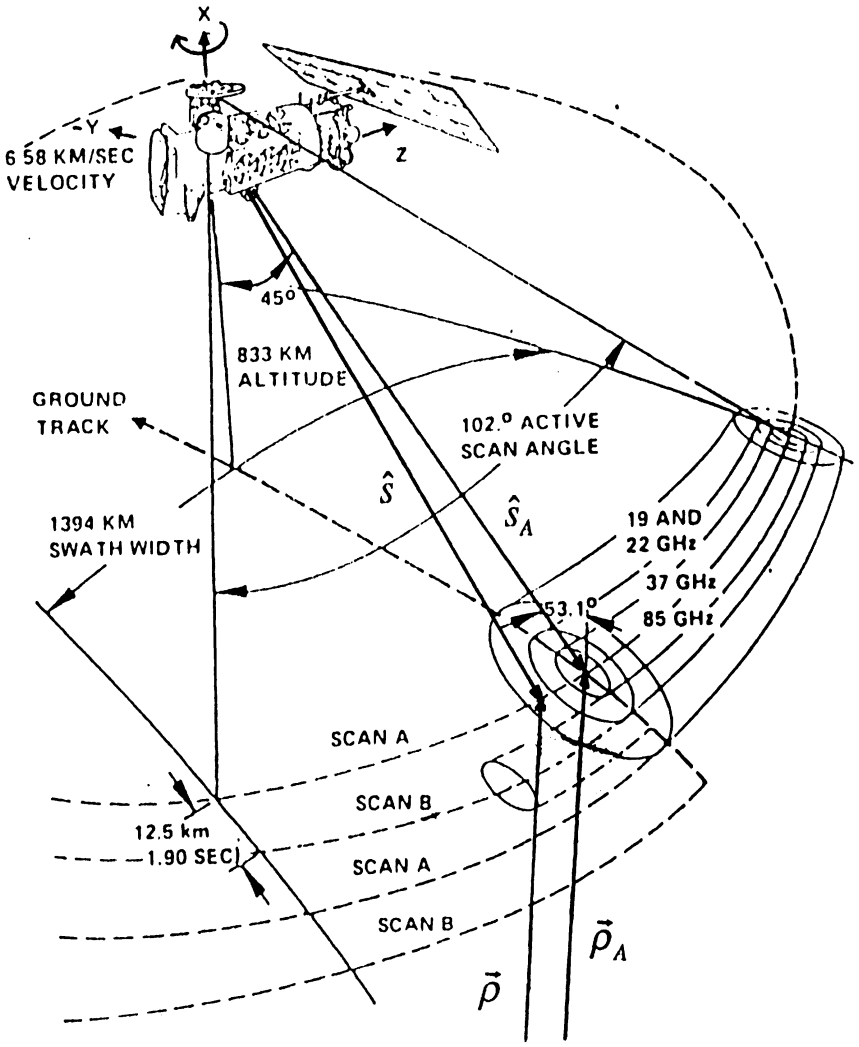

Figure 2. SSM/I scan geometry showing earth and satellite coordinate system reference vectors. $\vec{\rho}$ and $\vec{\rho}_A$ are normal to the earth's surface. (Modified from [5], Figure 2.8.)

where the vector $\vec{\rho}_A$ points from the center of the earth to the effective beam center on the earth's surface.

For simplicity, we will approximate the brightness temperature upwelling from an area *dA* as being both independent of direction and, on average, independent of time. This assumption constitutes a limitation in the analysis especially if the T_B at a particular *dA* changes significantly over the range of directions or times at which it is viewed by the radiometer. Nevertheless, for all practical purposes, the functionality of T_B simplifies to:

$$T_B(\vec{\rho},\hat{s}(t'),t') = T_B(\vec{\rho}) \tag{5}$$

Then T_B comes out of the time integral in (4) and we can define an effective antenna gain:

$$\overline{G}(\vec{\rho}_A,\vec{\rho}) = \frac{1}{\tau}\int_{-\frac{1}{2}}^{+\frac{1}{2}} dt' G(\hat{s}_0(t'),\hat{s}(t'))\left[\frac{-\hat{s}(t')\cdot\hat{\rho}}{s^2(t')}\right]. \tag{6}$$

Combining equations (4), (5) and (6) yields a simplified expression for the measured brightness temperature:

$$T_A(\vec{\rho}_A) = \iint_E dA\,\overline{G}(\vec{\rho}_A,\vec{\rho})\,T_B(\vec{\rho}) \tag{7}$$

Interpolation of the T_A to a higher sampling density is performed in the reference frame of the satellite measurements, i.e. interpolated data points are added along and between the swaths in columns parallel to the subsatellite track. Figure 3 shows this geometry for a set of samples midway between the middle and the end of the swath. To estimate the antenna temperature, $\tilde{T}_A(\vec{\rho}_d)$, which would have been measured by the sensor at an arbitrary location, $\vec{\rho}_d$, a weighted linear combination of a set of neighboring sensor measurements is used:

$$\tilde{T}_A(\vec{\rho}_d) = \sum_{i=1}^{N} a_i T_A(\vec{\rho}_{Ai}) \tag{8}$$

where the $\{a_i\}$ correspond to the set of measurements $\{T_A(\vec{\rho}_{Ai})\}$ and are the set of weighting coefficients to be determined.

Substituting (5) into (8) yields

$$\tilde{T}_A(\vec{\rho}_d) = \iint_E dA \sum_{i=1}^{N} a_i \overline{G}(\vec{\rho}_{Ai},\vec{\rho})\,T_B(\vec{\rho}) \tag{9}$$

and leads to a definition of the effective interpolated antenna gain function as:

$$\overline{G}_I(\vec{\rho}_d,\vec{\rho}) = \sum_{i=1}^{N} a_i \overline{G}(\vec{\rho}_{Ai},\vec{\rho}). \tag{10}$$

To determine the $\{a_i\}$, we would like to find a criterion which minimizes the error in the estimate of $T_A(\vec{\rho}_d)$:

$$\begin{aligned} e &= \left|T_A(\vec{\rho}_d) - \tilde{T}_A(\vec{\rho}_d)\right| \\ &= \left|\iint_E dA\left[\overline{G}(\vec{\rho}_d,\vec{\rho}) - \overline{G}_I(\vec{\rho}_d,\vec{\rho})\right]T_B(\vec{\rho})\right|. \end{aligned} \tag{11}$$

It is clear from (11) that e will be minimized if $\overline{G}$ is closely approximated by the interpolated pattern, $\overline{G}_I$—certainly a desirable condition if beam integrity is to be retained in the resampling process. As in [1] and [2], the solution for the weighting coefficients $\{a_i\}$ is obtained by minimization of Q_d:

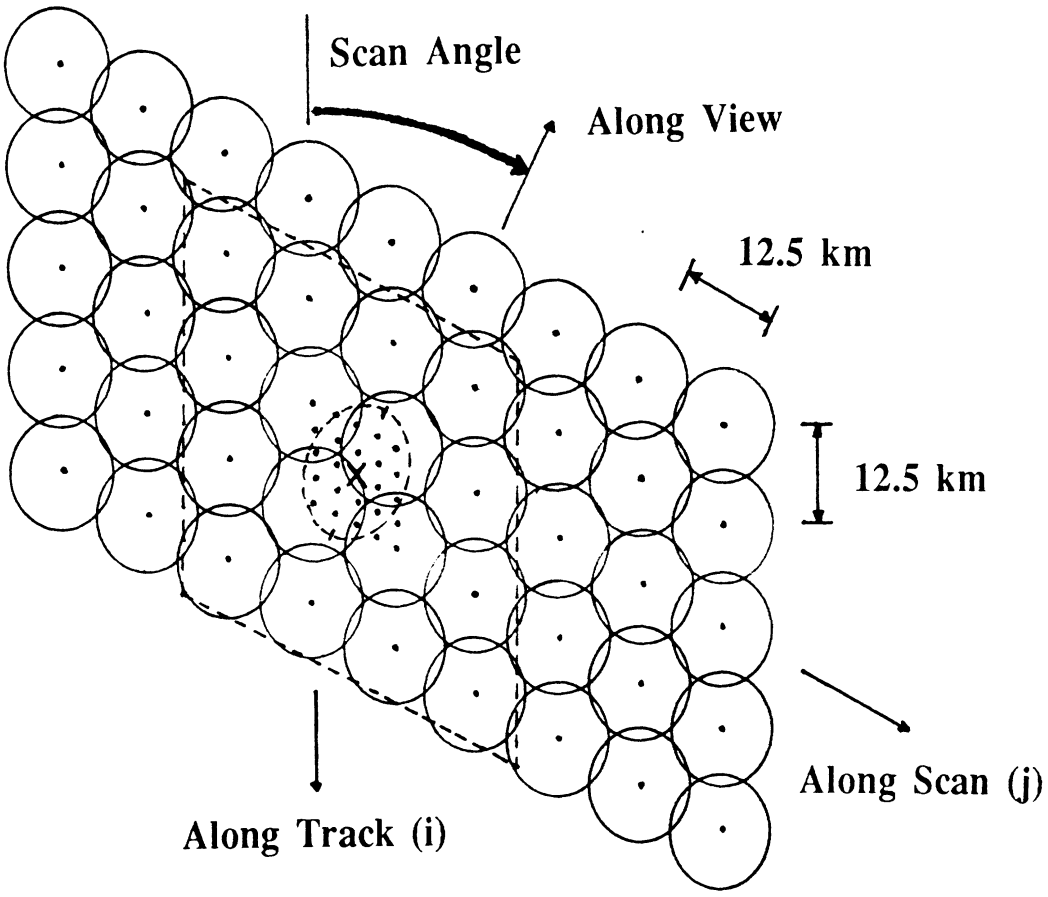

Figure 3. SSM/I measurement geometry. Measurements are represented by circles approximating the 3 dB beam diameter of the 85 GHz radiometer. The boxed measurements are used to calculate the antenna temperature at the interpolation points marked with dots. The optimal interpolated beam pattern of the point marked with an X is represented by the dashed ellipse. The scan angle is approximately 27° past the subsatellite track point.

$$Q_d = \iint_E dA \left[\overline{G}(\vec{\rho}_d, \vec{\rho}) - \sum_{i=1}^{N} a_i \overline{G}(\vec{\rho}_{Ai}, \vec{\rho}) \right]^2 J(\vec{\rho}_d, \vec{\rho}) \tag{12}$$

where the function $J(\vec{\rho}_d, \vec{\rho})$ can be used, for example, to reduce the sidelobe levels in the optimal $\overline{G}_I$ but is set to unity in this analysis.

The $\{a_i\}$ which minimize Q_d are then given by [1]:

$$\vec{a} = g^{-1} \left[\vec{v} + \frac{\left(1 - \vec{u} g^{-1} \vec{v}\right)}{\vec{u}^T g^{-1} \vec{u}} \vec{u} \right] \tag{13}$$

where the components of the matrix g and the vectors $\vec{u}$ and $\vec{v}$ are given by:

$$g_{ij} = \iint_E dA\,\overline{G}(\vec{\rho}_{Ai},\vec{\rho})\overline{G}(\vec{\rho}_{Aj},\vec{\rho}) \tag{14}$$

$$u_i = \iint_E dA\,\overline{G}(\vec{\rho}_{Ai},\vec{\rho}) \tag{15}$$

$$v_i = \iint_E dA\,\overline{G}(\vec{\rho}_{Ai},\vec{\rho})\overline{G}(\vec{\rho}_{d},\vec{\rho}) \tag{16}$$

The solution for the $\{a_i\}$ is described in additional detail in [1], where minimization of Q_d is coupled with the minimization of the variance of the sensor noise in the estimate (9). Since system noise is not considered here, the variance in the resulting interpolated antenna temperatures must be examined to insure that it does not exceed acceptable levels. In this report, the noise in the sensor antenna temperature of each measurement is assumed to be uncorrelated and equal so that the resulting variance in the interpolated antenna temperature is given by:

$$\left(\Delta\tilde{T}_A\right)^2 = \vec{a}^T E\vec{a} = \left(\Delta T_A\right)^2 \sum_{i=1}^{N} a_i^2 \tag{17}$$

where E is the covariance matrix of measurement noise for the samples contributing to $\tilde{T}_A(\vec{\rho}_d)$.

3.2.2. Implementation

As an example of the interpolation and resampling process, a set of coefficients was computed for the geometry of the 85 GHz channels of the SSM/I. Since the calculation of the $\{a_i\}$ for some arbitrary $\vec{\rho}_d$ is not a computationally trivial task, a collection of coefficients was developed for interpolation to points fixed with respect to the SSM/I along-swath/along-track reference system. This reference system is shown schematically in Figure 3. A total of 2,048 coefficient sets were calculated yielding a four-fold increase in the 85 GHz sample density in each direction. The interpolated points, (i,j), are numbered from 1 to 512 in the along scan direction and from 1 to 4 in the along track direction. Only four rows of coefficients need be calculated since every fourth interpolated row of data has the same set of interpolation coefficients. Sixteen samples were used to calculate the antenna temperature at each interpolation point. For example, the samples used to interpolate to the point marked with the X in Figure 3 are delineated by the dashed box. In the calculation of the interpolation coefficients, the along-view and along-scan directions were assumed to be invariant over the area of the integration encompassing the 16 samples.

A brief summary of the SSM/I operational parameters necessary for the calculation of coefficients for the 85 GHz channels is given in Table 2. Since the measured antenna pattern was not available, we assumed a Gaussian beam pattern. The pattern was calculated using the 3dB beam widths (IFOVs) listed in [5]. These yielded the 3dB effective fields of view (EFOVs) given below. Note that the E-polarized plane of the

Table 2. SSM/I operational parameters relevant to the 85 GHz channels [5] and the EFOV's of the assumed beam pattern.

Parameter	Value
Altitude	833 km
Active scan angle	102.4°
Swath width	1394 km
Elevation along beam	1261 km
E-plane 3dB IFOV	0.42°
H-plane 3dB IFOV	0.45°
Incidence angle of beam	53.1°
Sample spacing	12.5 km
Spacing between swaths	12.5 km
Integration time	3.89 ms
Time between samples	4.22 ms
E-plane 3dB EFOV	15.5 km
H-plane 3dB EFOV	13.5 km

antenna pattern lies in the along view direction and the H-polarized plane lies in the along scan direction.

Table 3 presents three sets of interpolation coefficients corresponding to the columns (j) and rows (i) indicated. All three interpolation points fall midway between samples and midway between swaths as shown in Figure 3. The RMS noise factor is also given and is equal to the square root of the sum of squares of the a_i as used in equation

Table 3. Interpolation coefficients at the indicated column and row. See Figure 3 for an example of measurement orientation. Ordering of weighting coefficients is the same as ordering of samples—left to right, top to bottom.

```
Column =  27, Row = 3, RMS noise factor = 0.87:
     -.11291   -.01291    .00089    .00621
     -.01547    .60375    .02664    .00380
      .00380    .02664    .60375   -.01547
      .00621    .00088   -.01291   -.11291

Column = 255, Row = 3, RMS noise factor = 0.85:
      .05803   -.11472   -.11470    .05803
     -.08722    .39391    .39387   -.08721
     -.08721    .39387    .39391   -.08722
      .05803   -.11470   -.11472    .05803

Column = 355, Row = 3, RMS noise factor = 0.83:
      .01426   -.01739   -.07876   -.03757
     -.00116    .15475    .55088   -.08503
     -.08503    .55088    .15475   -.00116
     -.03757   -.07876   -.01739    .01426
```

(17). The coefficient set is symmetric because of the symmetries inherent in the assumed Gaussian antenna beam pattern. For the SSM/I beam patterns, we would expect the coefficients to exhibit such symmetries to at least first order.

The interpolated SSM/I data in the satellite coordinate system are shown in Figure 4 for an 85 GHz scene of eastern North America. The gray scale represents brightness temperatures from 167 K (white) to 270 K (black). The original data are shown in Figure 5. Notable features include the distinct islands and river systems along the Atlantic coast which are clearly distinguishable in the interpolated image of Figure 4. The occurrence of "bad data" in the upper left hand quadrant of the original image can be seen to corrupt neighboring pixels in the interpolated image, but there are otherwise no discernable artifacts of the interpolation process.

As a check of the accuracy of the resampling process, the interpolation process was repeated using points in the interpolated image as original data. Interpolated data points which fell midway between the original measurement points were used to recover data at points on the original grid by the interpolation method described above. We assumed as an approximation that the same coefficient set applied, although the geometry was slightly skewed. In comparing the original and recovered data, the average absolute deviation in brightness temperature from the original to the twice-interpolated image was 0.79 K, with outliers occurring in regions where sharp dark to bright boundaries existed.

Figure 4. 85 GHz SSM/I interpolated image representing a four-fold increase in sample density. Shown in the SSM/I reference frame where horizontal is along scan and vertical is along track. Characteristics are the same as in Figure 5.

Figure 5. Original 85 GHz SSM/I image of eastern North America, shown in the SSM/I coordinate system (horizontal is along scan, vertical is along track); Jan. 23, 1989; Coloring: white=167K, black=269K.

3.3. Nearest-Neighbor Registration to MEG1b

The second component of the resampling process is the registration of the interpolated data to MEG1b points by nearest-neighbor association. The latitude and longitude coordinates of the interpolated data were calculated by bilinear interpolation of the latitude and longitude coordinates of the original data points. Because of the high density of the interpolated data, the largest error incurred through the registration process at 85 GHz is 1.1 km—only 9% of the 12.5 km spacing in the original data. Figure 6 shows the result of re-registering the interpolated data in Figure 4 to the appropriate section of the MEG1b database. The data has been scaled to byte format (numbers from 1 to 254) using the data's minimum and maximum values (approximately 167 to 269 K). The view in Figure 6 is essentially a section of a global Sinusoidal projection in which 0° longitude is the central meridian.

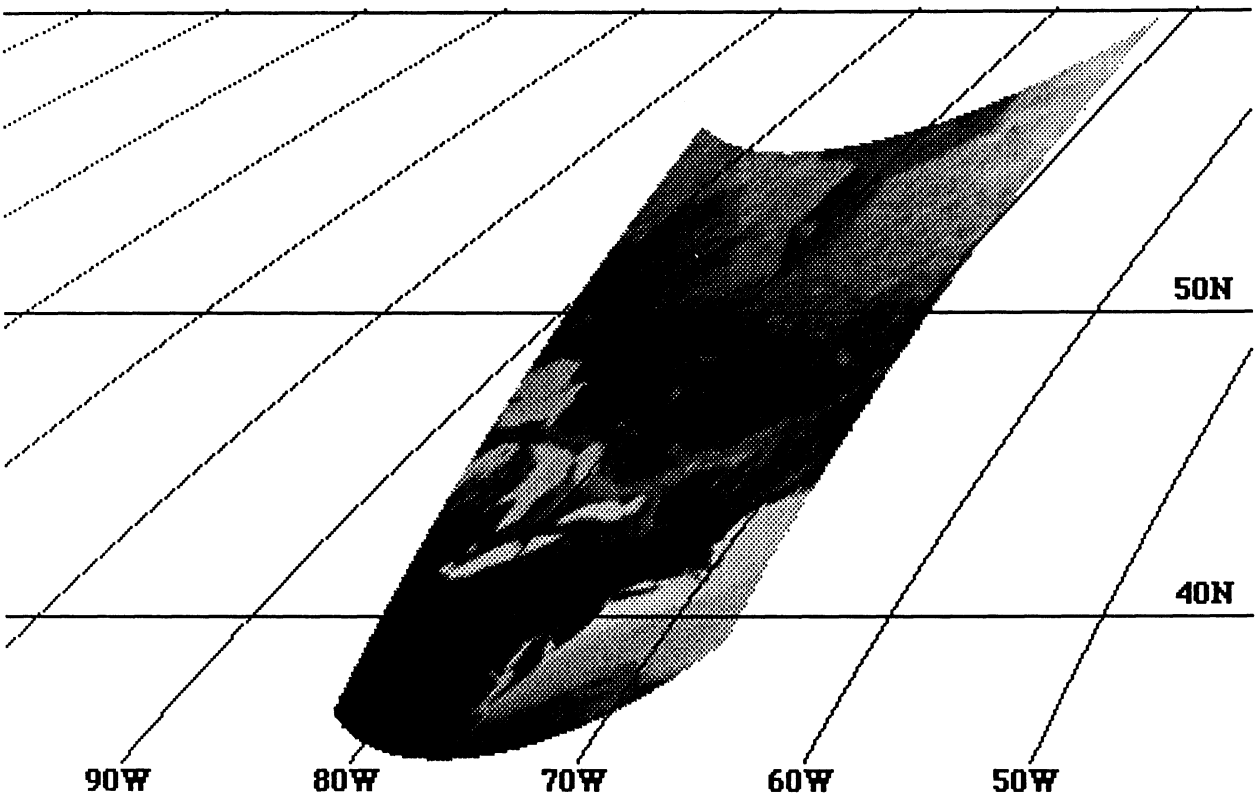

Figure 6. Interpolated data shown in Figure 4 re-registered to the appropriate part of the MEG1b grid.

4. Map Projections from MEG1b

The 0th column of every row in MEG1b is naturally aligned with the 0° meridian and therefore a Sinusoidal projection of the globe is readily made directly from MEG1b data. Regions on the projection far from the prime meridian, however, are displayed with increasing distortion, as demonstrated in Figure 7. Linear interpolation along the rows of data in MEG1b alone can be used to produce a number of convenient local projections. Spline interpolation was used in order to preserve as much as possible the underlying characteristics in the data.

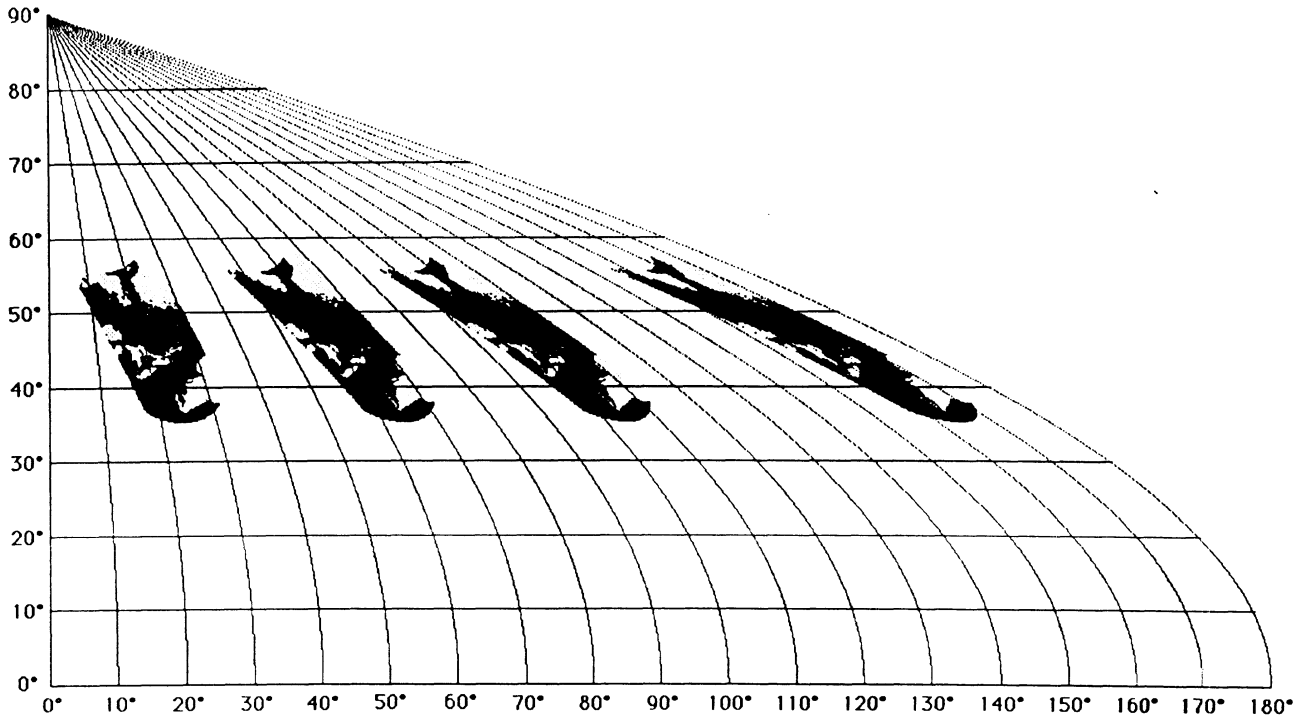

Figure 7. Example of shape distortion for regions far from the center of the MEG1b global Sinusoidal projection.

4.1. Local Sinusoidal Equal Area Projection

To produce a local Sinusoidal equal area projection, the location of each column in a row is shifted by a distance such that the first column of every row is aligned with a locally convenient meridian, as shown in Figure 8.

4.2. Plate Carree Conformal Projection

A Plate Carree conformal projection can be produced by mapping latitude and longitude linearly to the y and x coordinates, respectively, as in Figure 9. In this projection the equator and the meridians are true-length straight lines but there is significant length distortion along the parallels away from the equator.

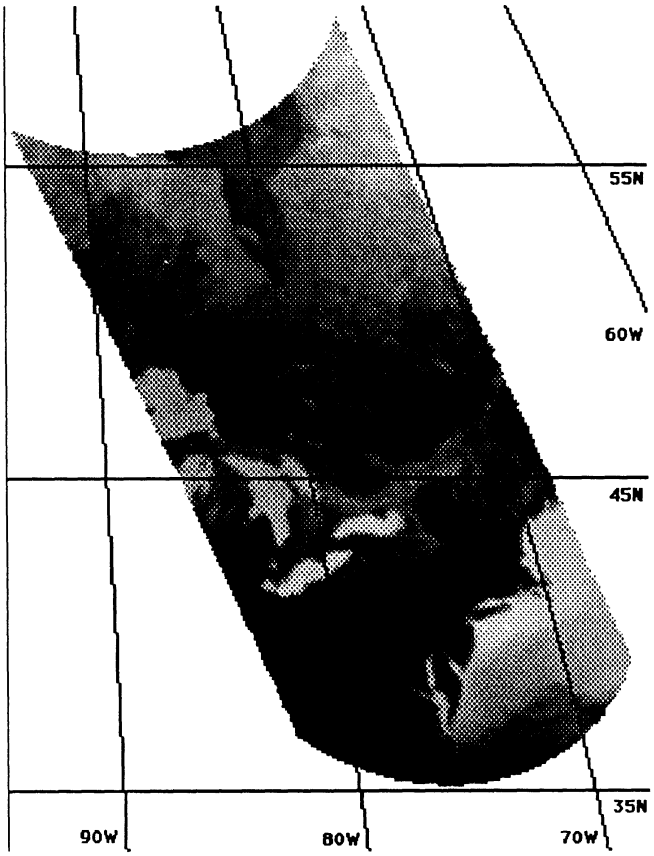

Figure 8. Example of a local Sinusoidal projection aligned on the 95W meridian.

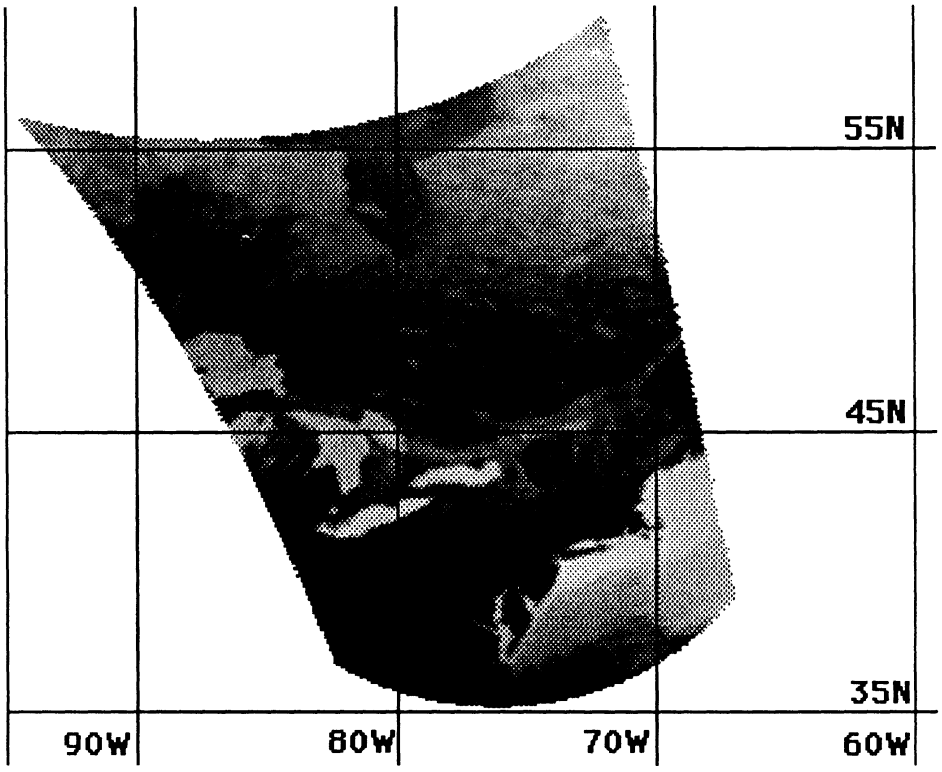

Figure 9. Example of a Plate Carree projection where meridians and the equator are true-length lines.

4.3. Carte Parallelogrammatique Projection

Similarly, a Carte Parallelogrammatique projection is produced by mapping latitude directly to the y coordinate while longitude is mapped to the x coordinate with a scaling factor equal to the cosine of some convenient latitude ($\pm\phi$). In this projection, the meridians and the $\pm\phi$ parallels are true-length lines. Figure 10 is an example of this projection with $\phi = 45°$.

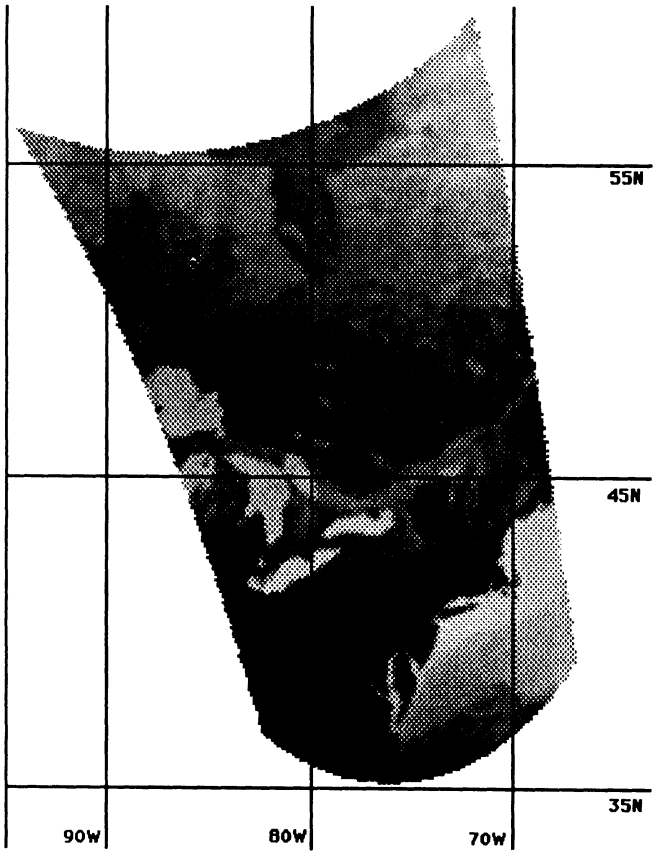

Figure 10. Example of a Carte Parallelogrammatique projection where the meridians and the 45° parallel are true-length lines.

5. Conclusions

The Michigan Earth Grid establishes a standard reference system for the earth which is easily visualized, manipulated and converted to local projections. The simple relationships between the related grid points of different radiometer channels provide the means to quickly estimate the gross spectral characteristics of grid cells, and the ease with which grid point coordinates are converted to latitude and longitude eliminates the need for space-consuming geolocation data.

The optimal interpolation technique described provides a way to resample SSM/I to the MEG1b database while retaining the spatial and spectral characteristics of the original data. By interpolating the data to four or more times its original density, the errors incurred

through nearest-neighbor registration can be minimized. Although calculation of the coefficients incurs high computational costs, interpolation to a satellite based reference frame means that these coefficients need be calculated only once.

References

[1] A. Stogryn, "Estimates of brightness temperatures from scanning radiometer data," *IEEE Trans. Antennas Propagat.*, vol. AP-26, pp. 720-726, Sept. 1978.

[2] G.A. Poe, "Optimum interpolation of imaging microwave radiometer data," *IEEE Trans. Geosci. Remote Sensing*, vol. GE-28, pp. 800-810, Sept. 1990.

[3] G.A. Poe and R.W. Conway, "A study of the geolocation errors of the Special Sensor Microwave/Imager (SSM/I)," *IEEE Trans. Geosci. Remote Sensing*, vol. GE-28, pp. 791-799, Sept. 1990.

[4] J. Hollinger et al., DMSP Special Sensor Microwave/Imager User's Guide, Naval Res. Lab., Washington, DC, 1987.